SPATIO-TEMPORAL ANALYSIS OF MANGROVE ECOSYSTEMS IN MUNCAR DISTRICT: IMPLICATIONS FOR BLUE CARBON CONSERVATION AND CLIMATE MITIGATION STRATEGIES

Hadiwijaya L. SALIM[1,3*], ROKHMATULOH[1], Burhanuddin ZEIN[2], Victor NIKIJULUW[2], Devi D. SURYONO[3], Anang D. PURWANTO[4], Yaya I. ULUMUDDIN[3], Bayu PRAYUDHA[3], Agustin RUSTAM[5], Early SEPTININGSIH[5], Joko PRIHANTONO[3], Mariska A. KUSUMANINGTYAS[3], Nasir SUDIRMAN[3], Restu N. A. ATI[3], Rita RACHMAWATI[5], Yusmiana P. RAHAYU[3], August DAULAT[3], Hanggar PRASETIO[2], Viga A. WICAKSONO[2] & Adi WIBOWO[1]

DOI: 10.21163/GT_2027.221.15

ABSTRACT

Mangrove ecosystems in coastal Indonesia, especially in Banyuwangi Regency, are facing pressure due to human activities and environmental changes. This study aimed to assess the spatio-temporal dynamics of mangroves and project changes in area and its implications for blue carbon stocks in Muncar District, Banyuwangi, from 2015 to 2030. A combination of Sentinel-2 data, multispectral Unmanned Aerial Vehicle (UAV) technology, and Cellular Automata–Markov (CA–Markov) modelling was used to map historical changes and project future conditions. Classification using the Baloloy algorithm showed a high level of accuracy (Overall Accuracy 98%, Kappa 0.96), with mangrove area increasing from 262.55 ha in 2015 to 309.90 ha in 2025. However, the CA–Markov scenario projection indicates a decrease in mangrove area to 275.38 ha by 2030, based on the transition dynamics derived from the 2015–2020 calibration period. The blue carbon stock estimation using a mean carbon storage value of 714 Mg C/ha (equivalent to 2,620 Mg CO_2-eq/ha), the projected 10.98-ha reduction relative to the simulated 2025 baseline corresponds to a potential reduction in mangrove carbon stock of approximately 7,840 Mg C (28,746 Mg CO_2-eq). This value represents potential carbon stock at risk associated with the projected reduction in mangrove areas rather than a direct estimate of atmospheric carbon emissions. Despite historical mangrove recovery, the results indicate continued vulnerability to future mangrove loss and associated reductions in landscape-scale carbon storage. Spatially targeted conservation, rehabilitation, and regular monitoring are therefore recommended to maintain mangrove extent and blue-carbon stocks and to support climate-change mitigation and coastal ecosystem resilience.

Keywords: *Mangrove; Blue Carbon; CA-Markov; Sentinel-2; Banyuwangi.*

---

[1] Universitas Indonesia, Department of Geography 16424, Depok, West Java, Indonesia; hadi026@brin.go.id (HLS), rokhmatuloh.ssi@sci.ui.ac.id (R), adi.w@sci.ui.ac.id (AW)

[2]Yayasan Konservasi Cakrawala Indonesia (YKCI) 12510, Jakarta, Indonesia; bburhanuddin@konservasi-id.org (BZ), Vnikijuluw@konservasi-id.org (VN), hprasetio@konservasi-id.org (HP), vanandawicaksono@konservasi-id.org (VAW)

[3] National Research and Innovation Agency (BRIN), Research Center for Ecology 16911, KST Soekarno, Cibinong, West Java, Indonesia; devi022@brin.go.id (DDS), yaya021@brin.go.id (YIU), bayu005@brin.go.id (BP), joko043@brin.go.id (JP), mari050@brin.go.id (MAK), nasi001@brin.go.id (NS), rest018@brin.go.id (RAA), yusm003@brin.go.id (YPR), augu001@brin.go.id (AD)

[4] National Research and Innovation Agency (BRIN), Research Center for Marine Aquaculture 83352, Lombok, West Nusa Tenggara, Indonesia; anan009@brin.go.id (ADP)

[5] National Research and Innovation Agency (BRIN), Research Center for Biota Systems 16911, KST Soekarno, Cibinong, West Java, Indonesia; agus183@brin.go.id (AR), earl002@brin.go.id (ES), rita013@brin.go.id

**Corresponding author: hadiwijaya.lesmana51@ui.ac.id*

1. INTRODUCTION

Mangroves serve as a fundamental socio-ecological bridge; they physically safeguard inland areas against seawater intrusion (Badriani et al., 2025) while simultaneously driving marine food web productivity and the viability of local fisheries (Azahra et al., 2024; Tanur et al., 2024). Indonesia represents a global epicenter for blue carbon ecosystems, harboring approximately 27% of the world's mangrove coverage, roughly 3.364 million hectares, and hosting 45 of the 75 known species globally (Bulan et al., 2023; Rahmandhana et al., 2022; Vitasari, 2015). As a primary component of blue carbon ecosystems, mangroves possess a high carbon sequestration capacity, with global estimates exceeding 22 million metric tons per year (Indriyani et al., 2020). Beyond climate change mitigation, they provide critical ecosystem services including coastal protection, sediment stabilization, and habitat provision for diverse coastal organisms (Blankespoor et al., 2016; Lam et al., 2023).

Despite their high ecological value, mangrove ecosystems globally are under significant pressure. The global mangrove area is estimated to have declined by 35% by the end of the 20th century (Bunting et al., 2020). In Indonesia, mangrove loss was recorded at 430,000 ha between 1985 and 2019, an average of approximately 12,647 ha per year (Arifianti et al., 2020). Various studies indicate that land conversion for aquaculture, settlements, industrial areas, and coastal infrastructure is the primary cause of mangrove degradation; this directly impacts biomass and carbon stocks both above and below ground (Salle et al., 2024; Richards & Friess, 2015).

In Banyuwangi Regency, particularly within the Muncar District, mangroves have faced persistent pressure due to the significant expansion of shrimp ponds (Pariyanto & Adamou, 2025). Anthropogenic activities such as logging, mangrove burning, and intensive cultivation have increased organic waste loads and deteriorated coastal water quality, which has ultimately reduced pond productivity and led to the abandonment of many sites. Furthermore, the loss of the mangroves' function as natural coastal protection has accelerated coastal erosion. Related spatial research in Muaragembong, Indonesia, has also examined the impacts of coastal erosion on land-cover changes to support coastal conservation planning (Solihuddin et al., 2024). While independent rehabilitation efforts have been underway since the late 1990s, following the 1994 tsunami, the dynamics of mangrove fluctuations in this region remain active. Consequently, comprehensive spatio-temporal studies are required to monitor these ongoing changes (Pariyanto & Adamou, 2025).

Previous studies have substantially improved the understanding of mangrove dynamics in Banyuwangi through various remote sensing and spatial analysis approaches. Rahmila et al., (2025) employed a Geographically Weighted Regression (GWR) model to reveal the spatial heterogeneity of environmental and anthropogenic drivers affecting mangrove distribution, while Hidayah et al. (2024) quantified long-term changes in mangrove extent in Pangpang Bay using multi-temporal satellite imagery. Likewise, Utomo et al., (2021) documented mangrove dynamics in Alas Purwo National Park using remote sensing techniques. These studies provide valuable information on historical changes and their driving factors. However, they primarily focus on retrospective analyses and do not incorporate predictive spatial modelling to anticipate future ecosystem trajectories. Furthermore, the implications of projected mangrove changes for blue carbon storage have not been explicitly evaluated, limiting their contribution to long-term climate mitigation planning.

Remote sensing has become an essential tool for monitoring mangrove ecosystems across Indonesia and Southeast Asia. In Indonesia, Beselly et al., (2021) demonstrated the advantages of integrating UAV and satellite imagery to improve the monitoring of mangrove and mudflat dynamics, while Kauffman and Donato, (2012)established standardized protocols for quantifying mangrove biomass and carbon stocks that are now widely adopted in blue carbon studies. At the regional and global scales, Yang et al., (2024) successfully applied UAV multispectral and hyperspectral imagery for fine-scale mangrove species classification, whereas Walcker et al., (2018) highlighted the temporal dynamics of blue carbon accumulation in mangrove ecosystems. Meanwhile, CA–Markov modelling has been extensively applied for predicting future land-use and land-cover changes (Gao et al., 2023; Lukas et al., 2023), but its application to mangrove ecosystems remains relatively limited. More importantly, studies integrating long-term Sentinel-2 monitoring, high-resolution UAV validation, predictive CA–Markov modelling, and blue carbon assessment within a single analytical

framework are still scarce, particularly at the local coastal management scale in Indonesia and Southeast Asia.

This study integrates multi-temporal Sentinel-2 imagery, multispectral UAV observations, CA–Markov spatial modelling, and blue carbon assessment into a unified framework for analysing mangrove dynamics in Muncar District, Banyuwangi. Sentinel-2 imagery provides consistent long-term monitoring of mangrove extent, while UAV observations are used to validate contemporary ecosystem conditions at very high spatial resolution. The validated mangrove maps are subsequently incorporated into a CA–Markov model to project future changes in mangrove distribution, and these projected changes are translated into potential blue carbon gains and losses. This study provides a more comprehensive framework for supporting sustainable mangrove management and evidence-based climate mitigation planning by combining historical mapping, predictive spatial modelling, and ecosystem service assessment within a single workflow

Based on these research gaps, this study aims to analyze the spatio-temporal dynamics of mangroves in Muncar, Banyuwangi, from 2015 to 2025 using Sentinel-2 imagery, validate current ecosystem conditions through multispectral UAV data, and project future changes using the CA–Markov approach. Furthermore, these fluctuations in mangrove area are linked to blue carbon storage dynamics to identify potential risks and opportunities for climate change mitigation. This integrated approach is expected to complement existing literature by providing a more anticipatory scientific framework for sustainable coastal planning and management in the region.

2. STUDY AREA

This research was conducted in the coastal zone of Muncar District, Banyuwangi Regency, East Java (**Fig. 1**), an area characterized by high mangrove dynamics resulting from pressures such as aquaculture expansion, urban settlement, and coastal rehabilitation efforts.

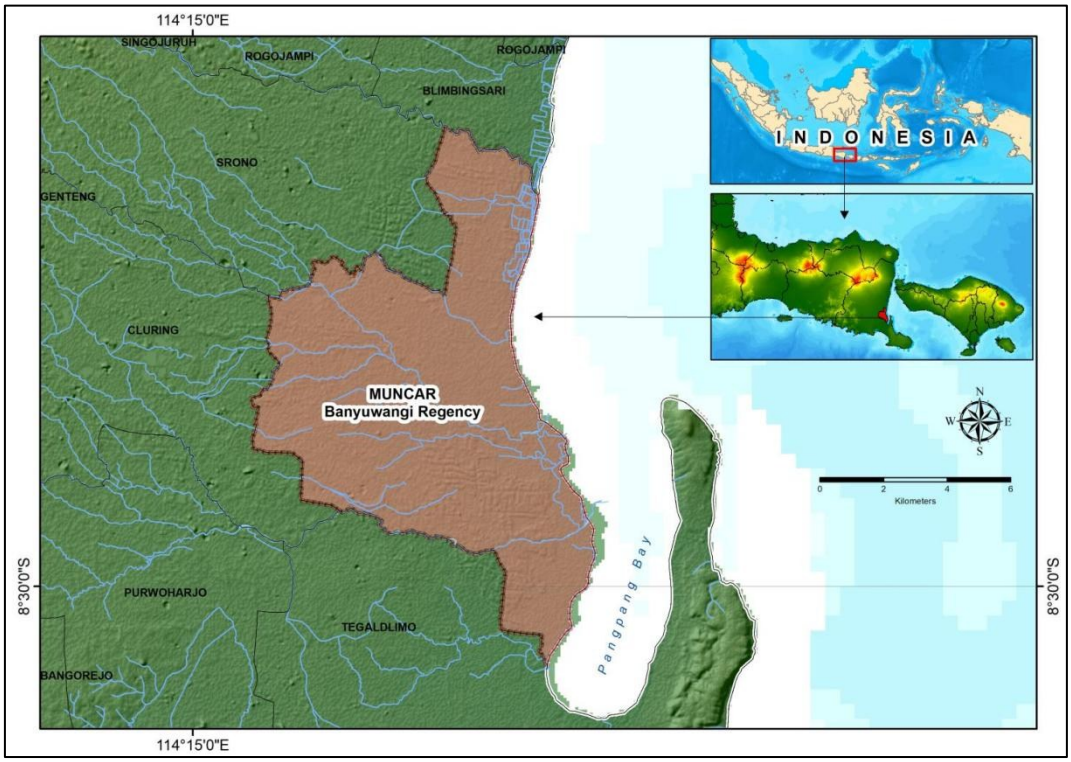


Fig. 1. Research study at Muncar District, Banyuwangi Regency, East Java Province.

This site was selected because it exemplifies the intense fluctuations in mangrove cover observed over the last decade, making it highly relevant for blue carbon analysis and spatial projections. Significant changes in mangrove extent have been documented across Banyuwangi; for instance, Pangpang Bay experienced a decline from 1,614.09 ha in 1994 to 1,465.83 ha in 2019. This trend is primarily driven by land conversion for fishponds and settlements, although localized rehabilitation programs have successfully expanded the cover in areas such as Alas Purwo, which increased from 383.01 ha in 2015 to 410.43 ha by 2020 (Hidayah et al., 2024; Utomo et al., 2021; Rahmila et al., 2025).

3. DATA AND METHODS

3.1. Satellite and UAV Data

Mangrove dynamics were analysed using Sentinel-2 Multispectral Instrument (MSI) imagery accessed through Google Earth Engine (GEE) for three observation years (2015, 2020, and 2025). Sentinel-2 Level-1C imagery was used for 2015, while Surface Reflectance imagery from the Harmonized Sentinel-2 collection (COPERNICUS/S2_SR_HARMONIZED) was used for 2020 and 2025. Images were filtered using a cloud-cover threshold of less than 20%. Cloud and cirrus contamination were removed using the QA60 quality band, specifically the cloud and cirrus bit masks. Sentinel-2 digital values were scaled by dividing by 10,000 to obtain surface reflectance values. The resulting images were composited using a median reducer and clipped to the study-area boundary. The Sentinel-2 bands used for mangrove mapping had a spatial resolution of 10 m. The resulting MVI-based classification was subsequently subjected to visual inspection and manual editing to remove obvious false-positive detections, particularly isolated patches occurring offshore and within aquaculture ponds where mangrove vegetation was clearly absent.

For the 2025 assessment, multispectral UAV imagery was additionally used to support validation of the satellite-derived mangrove classification. The UAV imagery was acquired using a DJI Phantom 4 Multispectral at an approximate flight altitude of 100 m on 6 and 7 August 2025. The resulting high-resolution multispectral imagery was used as reference data for validation of the 2025 mangrove classification. Ancillary spatial datasets were incorporated into the subsequent spatial analysis and modelling. River networks, roads, and settlement data were obtained from the Indonesian Geospatial Information Agency (Badan Informasi Geospasial—BIG) in vector format and subsequently converted to 1-m raster data for spatial modelling. A digital elevation model (DEM) obtained from BIG, with a spatial resolution of 8 m, was also incorporated into the spatial modelling. These ancillary datasets were used to represent environmental and anthropogenic spatial factors associated with mangrove-land-cover transitions (**Table 1**).

Table 1.

Spatial and ancillary dataset used in the study

Dataset	Source	Format	Spatial resolution	Function
Sentinel-2 MSI imagery	Google Earth Engine	Raster	10 m	Mangrove classification
Multispectral UAV imagery	Field survey	Raster	<10 cm	2025 classification validation
River network	BIG	Vector → raster	1 m	Spatial modelling
Roads	BIG	Vector → raster	1 m	Spatial modelling
Settlements	BIG	Vector → raster	1 m	Spatial modelling
Digital Elevation Model (DEM)	BIG	Raster	8 m	Spatial modelling

3.2. Image pre-processing in Google Earth Engine

Sentinel-2 image preprocessing was conducted on the Google Earth Engine (GEE) platform using the JavaScript API. The processing sequence comprised image collection filtering, cloud and cirrus masking, reflectance scaling, annual median composite generation, and spatial clipping to the study-area boundary.

For the 2015 observation, Sentinel-2 Level-1C imagery from the Harmonized Sentinel-2 collection (COPERNICUS/S2_HARMONIZED) was filtered spatially to the Muncar study area and temporally according to the observation year. For the 2020 and 2025 observations, Sentinel-2 Surface Reflectance imagery from the Harmonized Sentinel-2 collection (COPERNICUS/S2_SR_HARMONIZED) was used with the same spatial and temporal filtering procedure. Images with a scene-level cloud-cover percentage of less than 20% were retained. Pixel-level cloud and cirrus contamination was subsequently masked using the QA60 quality band, with bits 10 and 11 representing cloud and cirrus contamination, respectively. The retained Sentinel-2 observations were scaled by dividing the digital values by 10,000 to obtain reflectance values.

For each observation year, the cloud-masked images were subsequently composited using the median reducer to generate an annual composite. The composite image was then clipped to the Muncar District boundary, which was provided as a vector polygon uploaded to GEE as a table asset. The resulting annual Sentinel-2 composites were used as input data for subsequent MVI-based mangrove classification.

3.3. Mangrove classification

Mangrove classification was performed using the Mangrove Vegetation Index (MVI) proposed by Baloloy et al. (2020). The index was selected to distinguish mangrove vegetation from surrounding land and water surfaces based on the spectral characteristics of mangrove canopies. For Sentinel-2 imagery, the Green, NIR, and SWIR1 bands corresponded to Bands 3, 8, and 11, respectively. Following the implementation in Google Earth Engine, the MVI was calculated as:

$$MVI = abs(NIR - Green) / abs(SWIR1 - Green) \quad (1)$$

where NIR represents Band 8, Green represents Band 3, and SWIR1 represents Band 11.

The absolute values were applied to both the numerator and denominator, consistent with the implementation of the index in the GEE workflow.

A threshold of MVI > 4.5 was used to identify mangrove pixels, while pixels with MVI $\leqslant$ 4.5 were classified as non-mangrove. The threshold was adopted from Baloloy et al. (2020) and was not locally recalibrated in the present study. To ensure temporal comparability, the same threshold and classification procedure were applied consistently to the 2015, 2020, and 2025 annual Sentinel-2 composites. The resulting binary classification was visually inspected and manually edited to remove obvious false-positive detections, particularly isolated patches occurring offshore and within aquaculture ponds where mangrove vegetation was clearly absent. The manually refined mangrove maps were subsequently used for mangrove-area estimation and multitemporal change analysis. To restrict the classification to areas potentially suitable for mangrove occurrence, inland areas and non-coastal water bodies were masked from the classification results. The accuracy of the final 2025 mangrove map was subsequently assessed using independently generated stratified random validation points, as described in Section 3.4.

3.4. Accuracy Assessment

The formal accuracy assessment was conducted for the 2025 mangrove classification using 100 independent validation points generated in ArcGIS using the Create Accuracy Assessment Points tool with an equalized stratified random sampling strategy. The validation points were not used to calibrate

the MVI threshold, because the threshold of 4.5 was adopted from Baloloy et al. (2020) and was not locally recalibrated in this study.

The equalized stratified design ensured that the validation sample represented the mangrove and non-mangrove classes in a balanced manner. At each validation location, the class assigned by the Sentinel-2 MVI classification was compared with the reference class interpreted from high-resolution imagery available through Google Earth and multispectral UAV imagery. The reference interpretation was used to determine whether each validation point represented mangrove or non-mangrove cover. The resulting reference and classified labels were summarized in a confusion matrix. Overall Accuracy (OA), Producer's Accuracy (PA), User's Accuracy (UA), and the Kappa coefficient were calculated to evaluate the agreement between the MVI-based classification and the reference data.

The formal accuracy assessment was limited to the 2025 classification because the available independent high-resolution reference data were associated primarily with the most recent observation period. Therefore, quantitative accuracy measures were not separately estimated for the 2015 and 2020 classifications. Their temporal comparability was instead supported by applying the same MVI formulation, threshold, and classification across all observation years. Consequently, uncertainty in the historical 2015 and 2020 classifications should be considered when interpreting the magnitude and spatial pattern of long-term change.

3.5. Change detection of Mangrove area and CA-Markov Modelling

Mangrove land-cover changes were quantified by comparing the binary mangrove maps derived from the 2015, 2020, and 2025 Sentinel-2 observations. Spatial changes were categorized into stable mangrove, mangrove gain (non-mangrove to mangrove), and mangrove loss (mangrove to non-mangrove). The resulting change maps were used to visualize the spatial distribution of mangrove persistence, gain, and loss, while mangrove-area dynamics were quantified for each village within Muncar District. The 2015 and 2020 mangrove maps were subsequently used as the initial and subsequent land-cover states, respectively, to calibrate the cellular automata (CA)–Markov model and simulate the mangrove distribution for 2025.

The CA–Markov modelling was implemented using the MOLUSCE plugin in QGIS. The 2015 mangrove map was specified as the initial land-cover state, while the 2020 mangrove map represented the subsequent land-cover state used to derive the transition probabilities. Four spatial variables were incorporated into the transition-potential modelling: digital elevation model (DEM), road network, settlement distribution, and river network. The river, road, and settlement datasets were converted from vector to 1-m raster format, while the DEM was provided as an 8-m raster dataset. Prior to transition-potential modelling, the correlation among the spatial variables was evaluated using Pearson's correlation coefficient.

Transition potentials were modelled using an Artificial Neural Network based on a Multi-Layer Perceptron (ANN-MLP). The CA configuration used a neighborhood size of 1 pixel, a learning rate of 0.2, a maximum of 1,000 iterations, six hidden layers, and a momentum value of 0.05. The calibrated transition-potential model was then combined with the Markov transition probabilities and cellular automata allocation procedure to generate the simulated 2025 mangrove distribution.

Model performance was evaluated by comparing the simulated 2025 mangrove distribution with the observed 2025 mangrove map derived independently from the Sentinel-2 classification. Model agreement was assessed using the percentage of correctness and Kappa-based measures, including overall Kappa, histogram Kappa, and location Kappa. These metrics were used to evaluate the agreement between the simulated and observed spatial distributions before the model was applied to the 2030 projection.

Following validation, the calibrated CA–Markov model was used to generate a scenario-based projection of mangrove distribution for 2030. The projection represents a continuation of the transition dynamics and spatial relationships learned from the historical 2015–2020 period and should therefore be interpreted as a model-based scenario rather than a deterministic prediction of future mangrove extent. The overall analytical workflow is summarized in **Fig. 2**

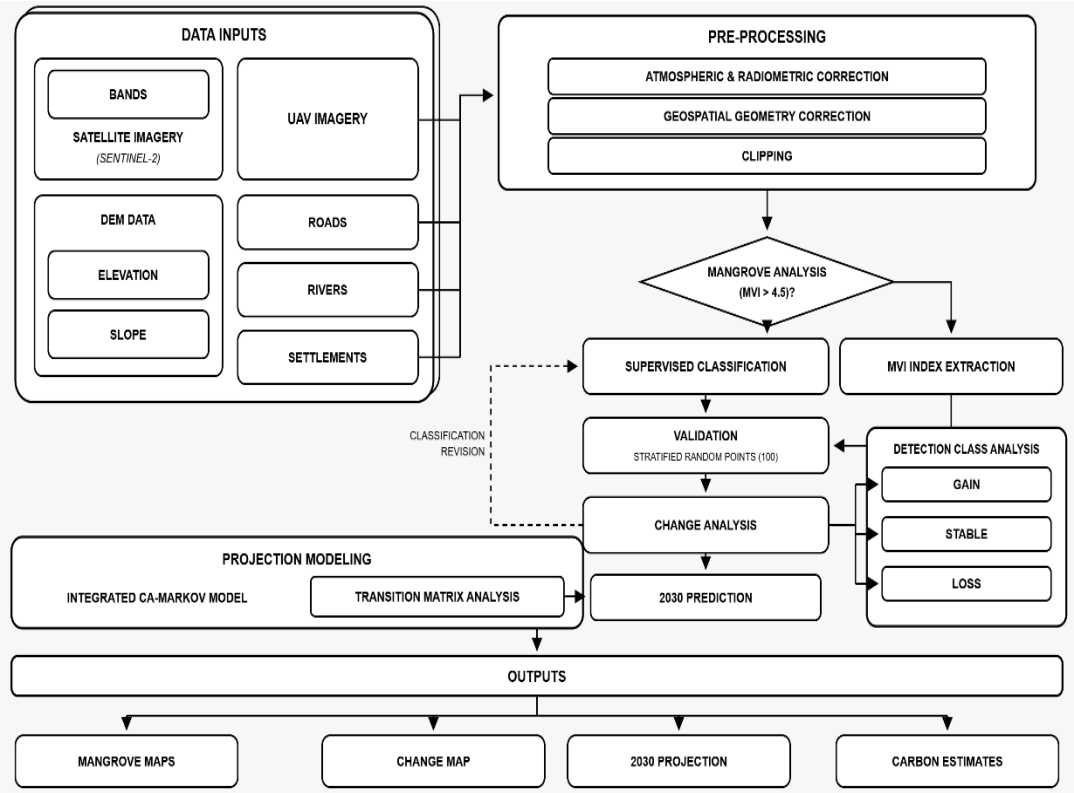


Fig. 2. Analytical workflow for mangrove mapping, change detection, CA–Markov modelling, hindcast validation, 2030 projection, and blue-carbon estimation.

3.6. Estimation of blue carbon dynamics

Measurements of mangrove biomass and sediment organic carbon following the field protocols of Kauffman and Donato (2012) were applied to estimate blue carbon stocks. Field sampling was conducted at five sites in Muncar District, Banyuwangi Regency. At each site, five circular plots (radius = 7m) were installed resulting in a total of 25 plots. Each circular plot covered approximately 154 m². In each plot, all mangrove trees were surveyed, and their Diameter at Breast Height (DBH) was recorded. Species identification was conducted in the field on site, whereas the species allometric equations, corresponding wood densities, and references used to estimate above-ground biomass are provided in **Table 2**.

Table 2.

Species allometric equation used for above-ground biomass estimation in Muncar mangroves.

Species	Equation	Wood density (ρ)	References
Bruguiera cylindrica	$0.0754\ \rho\ D^{2.505}$	0.8427	Clough and Scott,1989
Bruguiera gymnorhiza	$0.0754\ \rho\ D^{2.505}$	0.741	Clough and Scott,1989
Ceriops tagal	$0.251\ \rho\ D^{2.46}$	0.8859	Komiyama *et al. 2005*
Avicennia alba	$0.251\ \rho\ D^{2.46}$	0.6987	Komiyama *et al. 2005*
Rhizophora apiculata	$0.043\ D^{2.63}$	0.8814	Amira, 2008
Rhizophora mucronata	$0.128\ D^{2.60}$	0.8483	Fromard *et al*, 1998
Sonneratia alba	$0.3841\ \rho\ D^{2.101}$	0.6443	Cole *et. al.*, 1999; Kauffman & Cole, 2010

Subsequently, the above ground biomass data was converted to carbon stock using a carbon fraction of 0.5 calculated using the equation:

$$AGC = AGB \times 0.5 \quad (2)$$

Below ground biomass (BGB) was estimated using an allometric equation following Komiyama et al. (2005). The result was then converted into carbon by a conversion factor of 0.39.

$$BGB = 0.199\rho^{0.899}D^{2.22} \quad (3)$$

$$BGC = BGB \times 0.39 \quad (4)$$

where AGB is the above ground biomass (Mg ha-1), AGC is the above ground carbon (MgC ha-1), BGB is the below ground biomass (Mg ha-1), and BGC is the below ground carbon (MgC ha-1).

Sediment organic carbon was analysed using the Loss-on-Ignition (LOI) method. Soil cores were collected from eleven sampling points distributed across representative mangrove stands within the study area. At each sampling point, sediment cores were collected to a depth of 1 m using a soil corer. The samples were dried to constant weight and subsequently combusted in a furnace at 450°C for 4 h to determine organic matter loss using the LOI method. The percentage of organic matter was calculated as:

$$LOI\ (\%) = \frac{W1-W2}{W1} x\ 100 \quad (5)$$

where LOI is the percentage of organic matter (%), W_1 is the oven-dry sediment weight before ignition (g), and W_2 is the sediment weight after ignition (g).

The organic matter content obtained from the LOI analysis was converted to organic carbon (OC) using the Van Bemmelen conversion factor of 0.58, following the procedure described by Kauffman and Donato (2012):

$$OC(\%) = LOI(\%) \times 0.58 \quad (6)$$

Subsequently, sediment organic carbon stock (SOC) was calculated as:

$$SOC = \rho \times d \times \frac{OC}{100} \quad (7)$$

where SOC is sediment organic carbon stock (Mg C ha^{-1}), ρ is sediment bulk density (g cm^{-3}), d is sampling depth (cm), and OC is the organic carbon content (%).

Total ecosystem carbon stock was calculated as the sum of above-ground carbon, below-ground carbon, and sediment organic carbon. Following this, the total carbon reserves were converted into a carbon dioxide equivalent (CO_2-eq) by a conversion factor of 44/12 based on the ratio of CO_2 molecule mass towards carbon.

$$TC = AGC + BGC + SOC \quad (8)$$

$$CO_2eq = TC \times \left(\frac{44}{12}\right) \quad (9)$$

where TC is the total carbon, and SOC is the soil organic carbon.

Spatial blue carbon stocks were estimated by applying the average carbon density value derived from the August 2025 field survey and UAV-based biomass measurements (714 Mg C ha^{-1}) to the mapped mangrove area for each observation year. The application of drone-based observations for mangrove biomass estimation has also been demonstrated in Karimunjawa Islands (Salim et al., 2020). This approach enabled the quantification of total carbon storage and its temporal dynamics across the 2015, 2020, and 2025 mangrove distributions. Furthermore, the projected mangrove extent generated by the CA–Markov model for 2030 was integrated with the carbon density estimates to assess potential future changes in blue carbon stoc ks. All carbon stock estimates were subsequently converted into carbon dioxide equivalents (CO_2-eq) to provide a standardized metric for evaluating the climate change mitigation potential of the mangrove ecosystem.

Field measurements were presented as mean ± standard deviation (SD) to describe variability among sampling plots and indicate the uncertainty associated with carbon stock estimation. The application of a single mean carbon density value across the entire study area may introduce uncertainty because spatial variations in species composition, stand age, forest structure, and sediment characteristics were not fully represented. Therefore, the estimated blue carbon stocks should be interpreted as landscape-scale estimates rather than site-specific values. Future studies should increase sampling intensity and develop site-specific carbon density models to improve estimation accuracy.

4. RESULTS AND DISCUSSIONS

4.1. Mangrove area changes

Spatial analysis showed a continuous increase in mangrove extent in Muncar District during the observation period. The mapped mangrove area increased from 262.55 ha in 2015 to 285.79 ha in 2020, representing a net increase of 23.24 ha (8.85%), equivalent to an average increase of approximately 4.65 ha yr^{-1}. The mangrove area increased further to 309.90 ha in 2025, representing an additional increase of 24.11 ha (8.44%) relative to 2020. Overall, the mapped mangrove extent increased by 47.35 ha (18.03%) between 2015 and 2025. These findings indicate a significant phase of ecosystem recovery within the region during this interval, likely driven by successful rehabilitation initiatives and natural regeneration in abandoned aquaculture sites.

Spatially, the most extensive mangrove cover is concentrated in Wringinputih Village, which exhibited a consistent expansion from 260.41 ha in 2015 to 306.73 ha by 2025 (**Table 3**). This growth is primarily attributed to the village's strategic location at the confluence of the Setail and Bago rivers. The continuous influx of fluvial sediment facilitates the formation of new intertidal substrates in the estuary, creating optimal conditions for mangrove colonization and seaward progradation. Furthermore, the designation of the Setail River estuary as a primary site for government and community-led reforestation programs has significantly bolstered these natural expansion trends.

Table 3.
Distribution of mangrove area in Muncar District in 2015, 2020 and 2025 per village.

No.	Village	Year		
		2015	**2020**	**2025**
1	Wringinputih	260.41	283.38	306.73
2	Kedungringin	0.77	1.24	0.99
3	Sumbersewu	0.74	0.45	1.19
4	Kumendung	0.36	0.37	0.32
5	Tembokrejo	0.27	0.35	0.67
	Total	*262.55*	*285.79*	*309.9*

While other villages, such as Tembokrejo, Kumendung, Sumbersewu, and Kedungringin, have relatively small mangrove areas, the dynamics are quite diverse. There was a trend of increasing mangrove area in 2020, but then a decline (in Kedungringin and Kumendung). However, there are also consistent increases, such as in Tembokrejo Village. This indicates a significant interplay of anthropogenic and natural dynamics in these villages.

Overall, Muncar District has exhibited a significant expansion in mangrove extent, reflecting a decade of historical recovery and a sustained growth trend. However, notable spatial disparities exist in the distribution of these gains. This landscape-level imbalance is heavily influenced by localized drivers: while sediment-rich estuaries facilitate expansion, areas adjacent to intensive aquaculture experience persistent degradation. Such uneven distribution suggests that despite the net increase in area, the ecosystem remains fragmented and vulnerable to localized anthropogenic pressures. The spatial transitions of the mangrove ecosystem between 2015 and 2020 are illustrated in **Fig.3**. The dynamics within Muncar District are categorized into four distinct classes:

- *Stable Non-mangrove:* Areas that remained devoid of mangrove cover.
- *Mangrove Gain (Red):* Areas where non-mangrove land transitioned into mangrove cover, indicating successful recruitment or reforestation.
- *Mangrove Loss (Black):* Areas where previously existing mangroves were converted or degraded into non-mangrove land.
- *Stable Mangrove (Green):* Persistent mangrove areas that remained unchanged throughout the study period.

The analysis results presented in **Table 4** and **Fig.3** demonstrate that "Stable Mangrove" is the dominant class in Muncar District, particularly in Wringinputih Village, which maintains over 235 ha of persistent cover. This stability suggests a high degree of resilience against localized anthropogenic pressures. Furthermore, 50.87 ha of land transitioned from non-mangrove to mangrove, with the vast majority occurring in Wringinputih (49.03 ha) and a smaller portion in Kedungringin (0.74 ha). This recovery is largely attributed to targeted rehabilitation programs within abandoned aquaculture ponds in southern Muncar and natural colonization on newly formed intertidal substrates in the Setail River estuary.

Conversely, mangrove loss (mangroves to non-mangrove) totaled 27 ha, predominantly localized in Wringinputih (25.56 ha). Consequently, while Wringinputih serves as the primary hub for mangrove expansion, it also remains a focal point for degradation, resulting in a net gain of 23.47 ha for the village.

Table 4.
Mangrove land-cover transitions per village in Muncar District for the period 2015 – 2020.

Information	Village name					Grand Total
	Kedungringin	Kumendung	Sumbersewu	Tembokrejo	Wringinputih	
Mangrove to Mangrove	0.52	0.06	0.03	0	234.70	235.31
Mangrove to Non-mangrove	0.24	0.31	0.71	0.25	25.56	27.07
Non-mangrove to Mangrove	0.74	0.31	0.43	0.36	49.03	50.87

4.2. Accuracy Test

Based on the results of the accuracy test using the confusion matrix method with 100 test samples, the accuracy values and kappa coefficient values are presented in **Table 5** below.

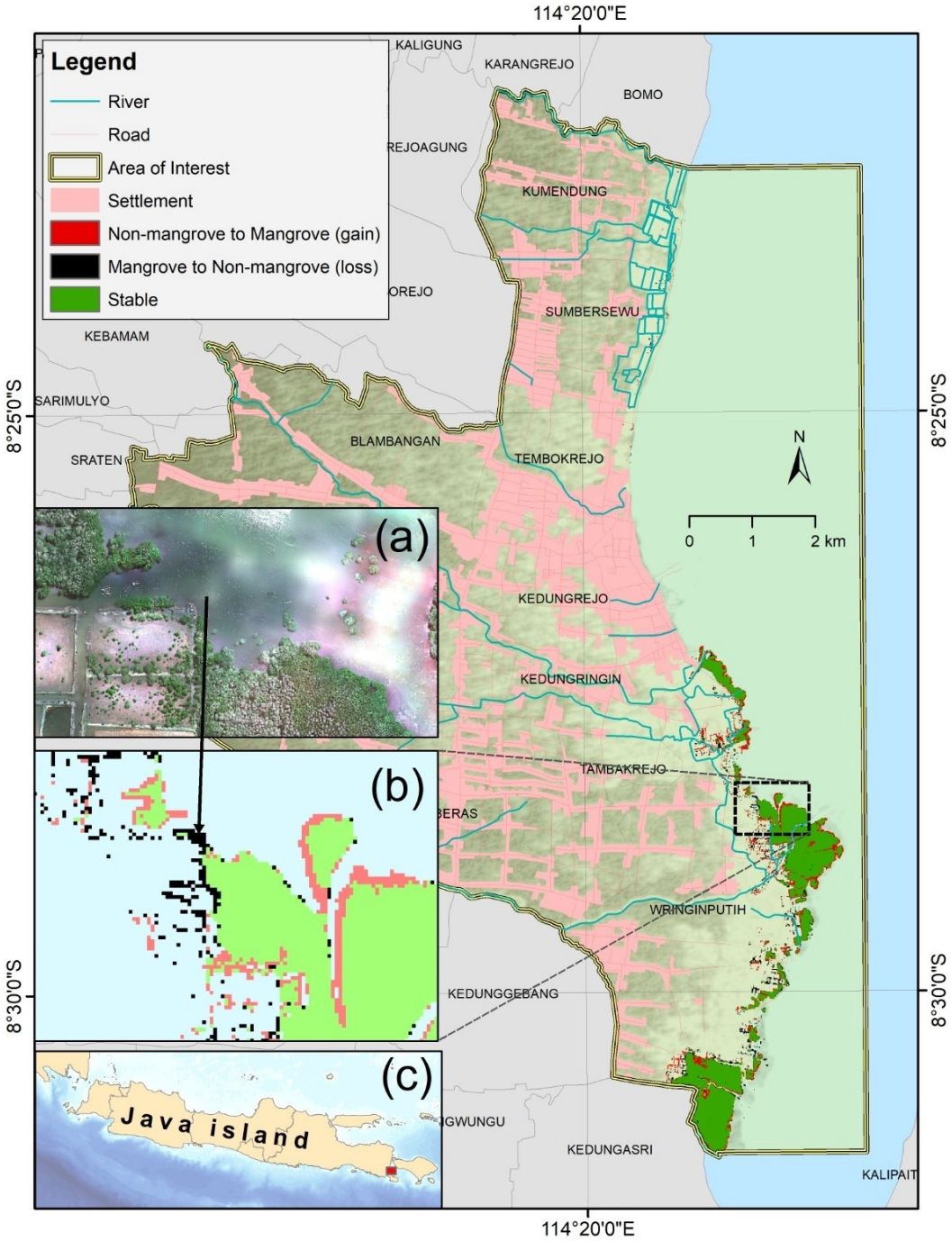


Fig. 3. Spatial distribution of mangrove changes in Muncar District, Banyuwangi, between 2015 and 2020. Green indicates stable mangrove, red indicates mangrove gain (non-mangrove to mangrove), and black indicates mangrove loss (mangrove to non-mangrove). (a) Orthophoto of UAV RGB image showing a representative mangrove area adjacent to shrimp ponds in Wringinputih Village, including areas of mangrove loss along pond margins. (b) Enlarged classified 2015–2020 change map corresponding to the UAV observation in panel (a), showing mangrove loss (black) along pond edges and mangrove gain (red) in newly colonized intertidal areas. (c) Location of the study area (red square) in Java, Indonesia.

Table 5.
Confusion matrix and accuracy assessment of the 2025 Sentinel-2 for mangrove classification

Class	Mangrove	Non-mangrove	Total	User's_Accuracy	Kappa
Mangrove	49.00	1.00	50.00	0.98	0.00
Non-mangrove	1.00	49.00	50.00	0.98	0.00
Total	50.00	50.00	100.00	0.00	0.00
Producer's_Accuracy	0.98	0.98	0.00	0.98	0.00
Kappa	0.00	0.00	0.00	0.00	0.96

The accuracy test results show a very high level of accuracy. Calculations using a confusion matrix show that the mangrove classification yields an Overall Accuracy of 98% and a Kappa coefficient of 0.96. This indicates a very strong match between the classification results and the reference data. The Producer's Accuracy and User's Accuracy values for the mangrove and non-mangrove classes each reached 98%, indicating minimal classification error and no systematic bias towards either class. These results indicate that the 2025 Sentinel-2 classification provided a reliable basis for estimating the contemporary mangrove extent and for evaluating the subsequent CA–Markov hindcast. However, the accuracy values should not be interpreted as direct quantitative accuracy estimates for the historical 2015 and 2020 classifications, for which independent accuracy assessment was not separately conducted.

4.3. Mangrove area predictions and blue carbon estimates for 2025 and 2030

The modelling results using the Cellular Automata-Markov method are presented in the following map (**Fig.4**).

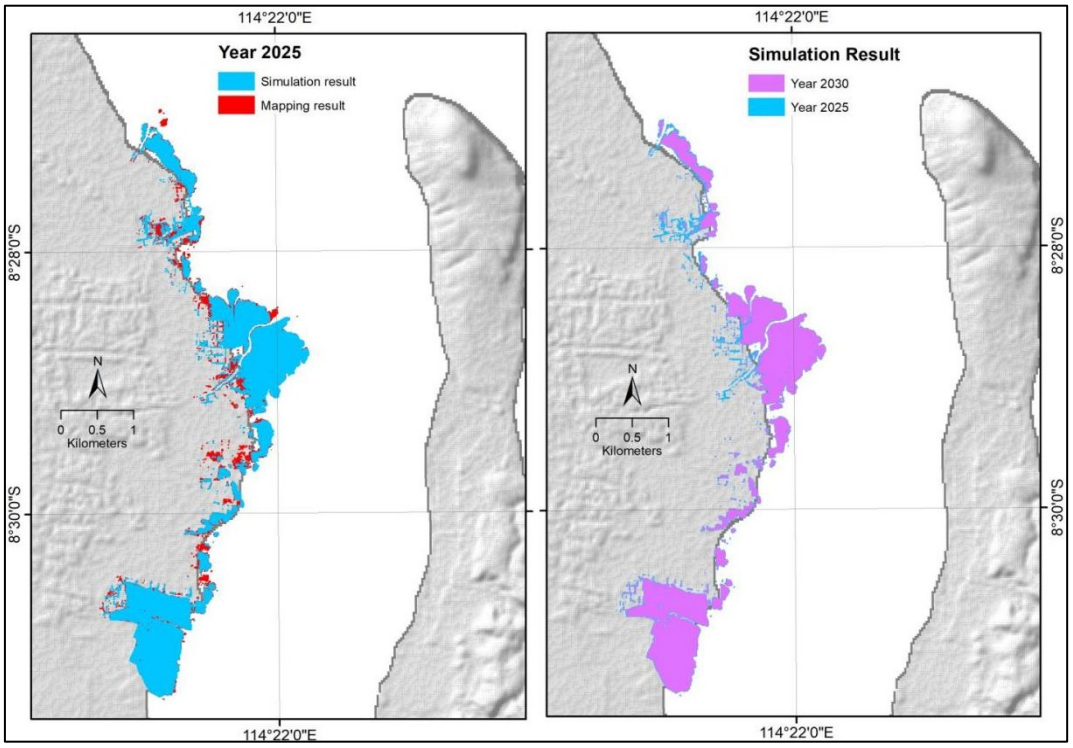


Fig. 4. The left panel compares CA-Markov simulation results (light blue) with mapping results (red), while the right panel shows changes in mangrove area from 2025 to 2030 based on the simulation results.

The CA–Markov model was calibrated using the 2015–2020 transition dynamics and subsequently used to hindcast the mangrove distribution for 2025. The observed 2025 mangrove map, derived independently from the Sentinel-2 MVI classification, was used as the reference for model validation. The observed mangrove extent in 2025 was 309.90 ha, whereas the CA–Markov hindcast produced 286.36 ha (**Table 6**). The difference was therefore 23.54 ha, corresponding to 7.60% of the observed 2025 mangrove area. This difference represents the discrepancy in total mapped area and was therefore complemented by spatial agreement assessment.

Table 6.

CA-Markov hindcast validation results for the 2025 mangrove distribution.

Validation measure	Value
Observed mangrove area, 2025	309.90 ha
Simulated mangrove area, 2025	286.36 ha
Area difference	23.54 ha
Difference relative to observed area	7.60%
Percentage correctness	99.514%
Kappa Simulation	0.93857
Overall Kappa	0.89952
Histogram Kappa	0.95782
Location Kappa	0.93913

This difference reflects the complexity of land use change dynamics that may not be fully captured by the model parameters, such as restoration interventions or local anthropogenic pressures. Nevertheless, the model has provided a strong basis for projecting change trends with sufficient reliability for initial planning purposes. Importantly, the area difference alone does not represent spatial agreement between the two maps. Therefore, the CA–Markov hindcast was further evaluated using Kappa-based spatial validation measures. The validation results yielded a percentage correctness of 99.51416%, with Kappa Simulation/current validation = 0.93857, Overall Kappa = 0.89952, Histogram Kappa = 0.95782, and Location Kappa = 0.93913. These metrics quantify the agreement between the simulated and observed 2025 spatial distributions.

The spatial agreement assessment further showed that 265.708 ha were correctly simulated as mangrove, while 44.615 ha of observed mangrove were not reproduced by the model (missed mangrove). Falsely simulated mangrove covered 20.445 ha, whereas 11,708.688 ha were correctly classified as non-mangrove by both datasets (**Fig. 5**). Based on the agreement-map assessment, the overall spatial agreement was 99.46%, while spatial disagreement accounted for 0.54% of the validation extent. The spatial distribution of correctly simulated, missed, and falsely simulated mangrove areas is illustrated in **Fig. 5**.

Following the hindcast validation, the calibrated CA–Markov model was used to project the mangrove distribution to 2030. The projected mangrove area decreased from 286.36 ha in the simulated 2025 state to 275.38 ha in 2030, corresponding to a reduction of 10.98 ha (3.83%) relative to the simulated 2025 baseline. The contrasting trajectories between the historical observations and the model projection reflect the different temporal bases of the two analyses. The observed mangrove area increased from 262.55 ha in 2015 to 309.90 ha in 2025, whereas the 2030 projection was generated from the 2015–2020 transition dynamics rather than from the observed 2020–2025 increase. Consequently, the projected decline represents the spatial outcome of continuing the transition dynamics derived from the 2015–2020 calibration period and should not be interpreted as a deterministic prediction of the actual future mangrove extent. This decline suggests that pressure on the mangrove ecosystem is predicted to continue without significant management intervention. Therefore, the results of this modelling can provide a scientific basis for developing more effective conservation policies, improving rehabilitation programs, and implementing regular monitoring to anticipate future degradation

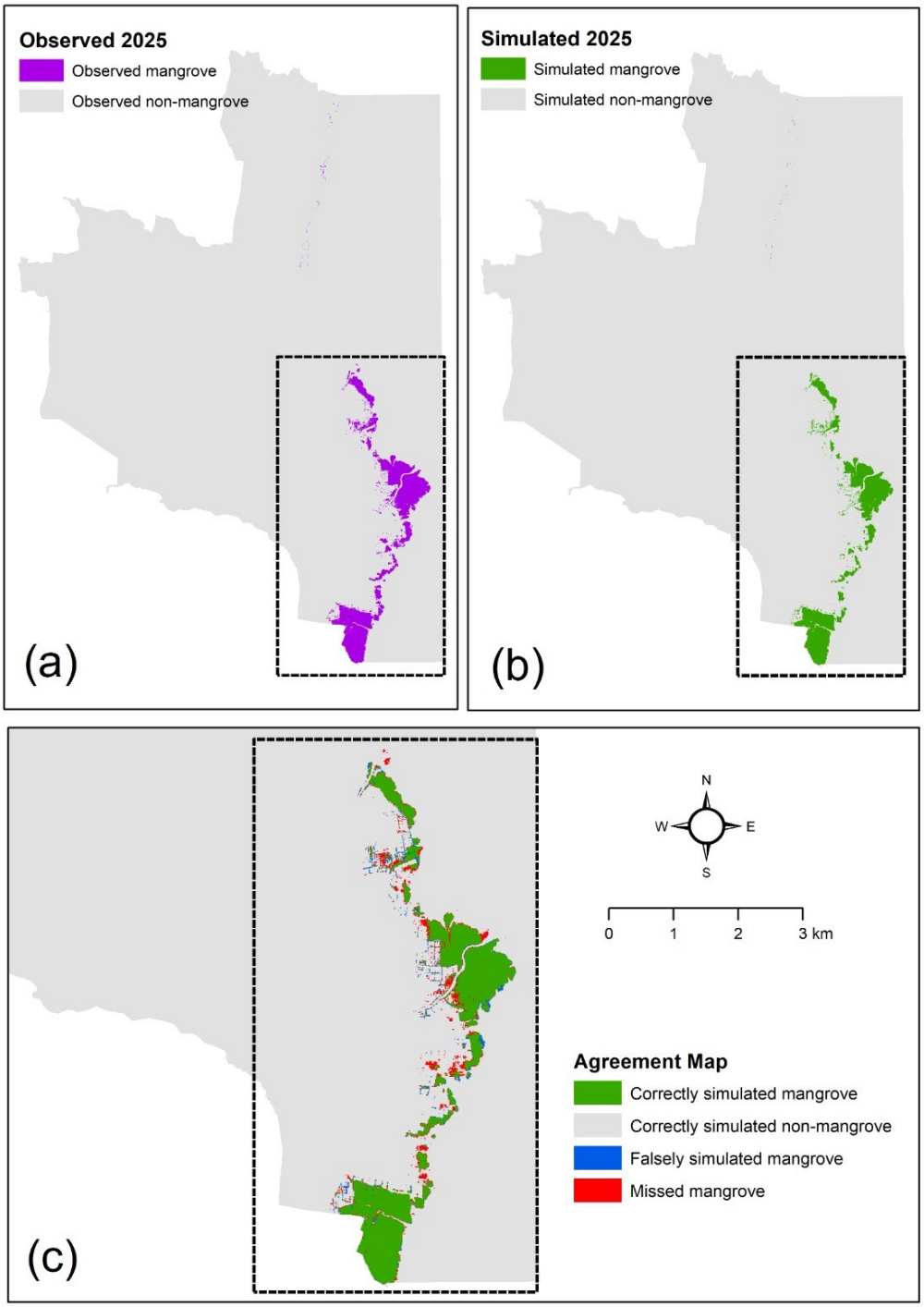


Fig. 5. Spatial validation of the CA–Markov hindcast for 2025. (a) Observed mangrove distribution derived from the Sentinel-2 MVI classification; (b) CA–Markov simulated mangrove distribution; and (c) spatial agreement between the observed and simulated 2025 maps, showing correctly simulated mangrove, correctly simulated non-mangrove, falsely simulated mangrove, and missed mangrove areas.

Although the projected decline represents less than 5% of the simulated 2025 mangrove area, even a relatively small reduction may be ecologically relevant because mangrove functions depend not only on total area but also on the persistence and spatial configuration of remaining stands. Therefore, the projected decline should be interpreted as a potential warning of localized degradation rather than as a negligible change in ecosystem condition. The modelling results can consequently support spatially targeted conservation, rehabilitation, and regular monitoring to identify areas that may become vulnerable to future mangrove loss.

The projected decline contrasts with the recovery observed during 2015–2025, but it is consistent with the premise that mangrove trajectories can vary across time according to changes in land-use pressure (Krauss et al., 2018), hydrological connectivity (López-Adame et al., 2026), sediment dynamics, and restoration interventions (Sidik et al., 2020). Previous studies have similarly shown that mangrove recovery at one period does not necessarily imply continued expansion under subsequent transition conditions. Mangrove is non-linear systems (Alongi, 2011), and influenced by human activities (Rasyid et al., 2016). In this context, the present projection should be interpreted as a spatial scenario derived from historical transition patterns rather than as evidence that future mangrove decline is inevitable

Based on the blue-carbon estimation, the mangrove ecosystem in Muncar represents an important landscape-scale carbon stock. Using the mean total carbon density of 714 Mg C ha^{-1} (equivalent to approximately 2,620 Mg CO_2-eq ha^{-1}) obtained from field surveys and UAV-supported measurements in August 2025, the observed mangrove extent of 309.90 ha in 2025 corresponds to an estimated carbon stock of approximately 221,269 Mg C, equivalent to approximately 812,000 Mg CO_2-eq. Using the simulated 2025 extent of 286.36 ha as the model baseline, the corresponding carbon stock is approximately 204,461 Mg C (approximately 749,000 Mg CO_2-eq). The difference between the observed and simulated estimates primarily reflects the underestimation of mangrove extent by the spatial simulation and illustrates the sensitivity of landscape-scale carbon estimates to mapped mangrove area.

The projected reduction to 275.38 ha by 2030 indicates a potential reduction in blue-carbon stock if the modelled transition dynamics continue. Assuming that the mean carbon density of 714 Mg C ha^{-1} remains constant, the projected 10.98-ha reduction from the simulated 2025 baseline corresponds to a potential reduction in mangrove carbon stock of approximately 7,840 Mg C, equivalent to approximately 28,746 Mg CO_2-eq. This value represents potential carbon stock at risk associated with the projected reduction in mangrove area and should not be interpreted as a direct estimate of atmospheric carbon emissions. Rather, mangrove degradation may reduce the ecosystem's capacity to retain carbon stored in biomass and sediments and may increase the risk of subsequent carbon release. Therefore, mangrove conservation and rehabilitation in Muncar District can contribute to both ecosystem resilience and climate-change mitigation by maintaining existing carbon stocks and reducing the potential for future carbon-stock losses.

5. CONCLUSIONS

This study revealed the spatio-temporal dynamics of the mangrove ecosystem in Muncar District, Banyuwangi Regency, by integrating multi-source remote sensing data with Cellular Automata–Markov (CA–Markov) modelling. The 2015–2025 period showed a positive recovery trend, with the observed mangrove area increasing from 262.55 ha to 309.90 ha. The recovery was particularly evident in Wringinputih Village, coinciding with areas associated with rehabilitation activities and favorable hydro-sedimentary conditions. Classification using the Baloloy algorithm applied to Sentinel-2 imagery achieved high accuracy, with an Overall Accuracy of 98% and a Kappa coefficient of 0.96. Hindcast validation of the CA–Markov model showed strong spatial agreement, including a Kappa Simulation of 0.93857, although the model underestimated the observed 2025 mangrove extent.

The CA–Markov scenario projection indicates a decline in mangrove area from 286.36 ha in the simulated 2025 baseline to 275.38 ha in 2030, corresponding to a reduction of 10.98 ha (3.83%). This projection is based on the transition dynamics derived from the 2015–2020 calibration period and

therefore represents a scenario of continued historical transition dynamics rather than a deterministic prediction of future mangrove extent. Assuming a mean carbon density of 714 Mg C ha^{-1}, the projected reduction corresponds to a potential reduction in mangrove carbon stock of approximately 7,840 Mg C, equivalent to approximately 28,746 Mg CO_2-eq. This value represents potential carbon stock at risk associated with the projected reduction in mangrove area and should not be interpreted as a direct estimate of atmospheric carbon emissions.

These findings highlight the importance of maintaining existing mangrove stands while strengthening spatially targeted rehabilitation in areas vulnerable to future loss. Integrating satellite-based monitoring, UAV-supported field validation, and spatial modelling can provide a practical basis for adaptive coastal management and for incorporating mangrove conservation and rehabilitation into local climate-change mitigation and ecosystem-resilience strategies.

REFERENCES

Alongi, D. M. (2011). Carbon payments for mangrove conservation: Ecosystem constraints and uncertainties of sequestration potential. *Environmental Science and Policy*, *14*(4), 462–470. https://doi.org/10.1016/j.envsci.2011.02.004

Arifanti, V., Kauffman, J., Ilman, M., Tosiani, A., & Novita, N. (2022). Contributions of mangrove conservation and restoration to climate change mitigation in Indonesia. Global Change Biology, 28(15), 4523-4538. https://doi.org/10.1111/gcb.16216

Azahra, R., Anggraini, P. K., Nuryasin, A., Hasan, H., & Nuryadin, D. F. E. (2024). Kondisi Ekosistem Mangrove Di Kawasan Ketapang Urban Aquaculture Berdasarkan Indeks Kesehatan Mangrove. Maiyah, 3(1), 1. https://doi.org/10.20884/1.maiyah.2024.3.1.11514

Badriani, R. E., Pramitasari, N., Sari, T. I., & Chaniago, R. Y. (2025). Sosialisasi Mitigasi Dampak Gelombang Tsunami Berbasis Ekosistem Mangrove di Pesisir Pantai Paseban. PEKAT: Jurnal Pengabdian Kepada Masyarakat, 4(2), 40-46. https://doi.org/10.37148/pekat.v4i2.66

Baloloy, A. B., Blanco, A. C., Sta. Ana, R. R. C., & Nadaoka, K. (2020). Development and application of a new mangrove vegetation index (MVI) for rapid and accurate mangrove mapping. ISPRS Journal of Photogrammetry and Remote Sensing, 166, 95–117. https://doi.org/10.1016/j.isprsjprs.2020.06.001

Beselly, S. M., Van Der Wegen, M., Grueters, U., Reyns, J., Dijkstra, J., & Roelvink, D. (2021). Eleven Years of Mangrove–Mudflat Dynamics on the Mud Volcano-Induced Prograding Delta in East Java, Indonesia: Integrating UAV and Satellite Imagery. *Remote Sensing*, *13*(6), 1084. https://doi.org/10.3390/rs13061084

Blankespoor, B., Dasgupta, S., & Lange, G. (2016). Mangroves as a protection from storm surges in a changing climate. Ambio, 46(4), 478-491. https://doi.org/10.1007/s13280-016-0838-x

Bulan, Dewi & Bestziel, Jheardy & Toufik, Julianti & Septiana, Yessi & Ashari, Devisa & Oktavianingsih, Okky & Savitri, Ratna & Fazar, Reza & Apriyana, Faidah & Khumairoh, Ai & S, Riski & Margareta, Fira & Ibrahim, Ibrahim. (2023). Optimalisasi Pengelolaan Ekowisata Hutan Mangrove "Lati Tuo" untuk Meningkatkan Perekonomian Warga Desa Klempang Sari. Jurnal Abdi Insani. 10. 2994-3004. 10.29303/abdiinsani.v10i4.1248.

Bunting, P., Rosenqvist, Å., Hilarides, L., Lucas, R., Thomas, N., Tadono, T., … & Rebelo, L. (2022). Global Mangrove Extent Change 1996–2020: Global Mangrove Watch Version 3.0. Remote Sensing, 14(15), 3657. https://doi.org/10.3390/rs14153657

Gao, C., Cheng, D., Iqbal, J., & Yao, S. (2023). Spatiotemporal Change Analysis and Prediction of the Great Yellow River Region (GYRR) Land Cover and the Relationship Analysis with Mountain Hazards. *Land*, *12*(2), 340. https://doi.org/10.3390/land12020340

Hidayah, Z., Rachman, H. A., & Wiyanto, D. B. (2024). Assessment of spatio-temporal dynamics of mangrove forest in Teluk Pangpang, Banyuwangi, East Java, Indonesia. *Biodiversitas*, *25*(7), 3138–3150. https://doi.org/10.13057/biodiv/d250736

Indriyani, L., Bana, S., Yasin, A., Sudia, L., Midi, L., & Hardin, H. (2020). The Potential of Blue Carbon Stocks and Carbon Dioxide Absorption in Mangrove Forests to Support Low Carbon Emission Development in Southeast Sulawesi Province, Indonesia. International Journal on Advanced Science Engineering and Information Technology, 10(6), 2526-2535. https://doi.org/10.18517/ijaseit.10.6.13332

Kauffman, J. B., & Donato, D. C. (2012). *Protocols for the measurement, monitoring and reporting of structure, biomass and carbon stocks in mangrove forests.* Center for International Forestry Research (CIFOR). https://www.cifor.org/publications/pdf_files/WPapers/WP86CIFOR.pdf

Krauss, K. W., Demopoulos, A. W. J., Cormier, N., From, A. S., McClain-Counts, J. P., & Lewis, R. R. (2018). Ghost forests of Marco Island: Mangrove mortality driven by belowground soil structural shifts during tidal hydrologic alteration. *Estuarine Coastal and Shelf Science*, *212*, 51–62. https://doi.org/10.1016/j.ecss.2018.06.026

Lam, K., Lam, Y., Ng, A., So, K., Tam, N., Lee, F., … & Mo, W. (2023). The Impact of Anthropogenic Pollution on Tidal Water Quality in Mangrove Wetlands. Journal of Marine Science and Engineering, 11(12), 2374. https://doi.org/10.3390/jmse11122374

López-Adame, H., Zaragoza-Méndez, F. Á., Lara-Domínguez, A. L., Alvarado-Barrientos, M. S., Mariño-Tapia, I., Sáinz-Hernández, E., Pérez-Ceballos, R., Zaldívar-Jiménez, A., & López-Portillo, J. (2026). Effectiveness of hydrological restoration in the mangrove of a coastal lagoon in the Gulf of Mexico. *Ecological Engineering*, *223*. https://doi.org/10.1016/j.ecoleng.2025.107848

Lukas, P., Melesse, A. M., & Kenea, T. T. (2023). Prediction of Future Land Use/Land Cover Changes Using a Coupled CA-ANN Model in the Upper Omo–Gibe River Basin, Ethiopia. *Remote Sensing*, *15*(4). https://doi.org/10.3390/rs15041148

Pariyanto, K. and Adamou, R. (2025). Sejarah Konservasi Mangrove Pantai Cemara, Kecamatan Muncar, Kabupaten Banyuwangi, 1980-an-2020. Aliansi Jurnal Hukum Pendidikan Dan Sosial Humaniora, 2(5), 178-188. https://doi.org/10.62383/aliansi.v2i5.1207

Rahmandhana, A. D., Kamal, M., & Wicaksono, P. (2022). Spectral Reflectance-Based Mangrove Species Mapping from WorldView-2 Imagery of Karimunjawa and Kemujan Island, Central Java Province, Indonesia. Remote Sensing, 14(1), 183. https://doi.org/10.3390/rs14010183

Rahmila, Y. I., Prasetyo, L. B., Kusmana, C., Basyuni, M., Pranoto, B., Rahmania, R., Halwany, W., Faubiany, V., Susantoro, T. M., Winarso, G., Efiyanti, L., & Indrawan, D. A. (2025). Spatial analysis of mangrove ecosystem dynamics in Banyuwangi: a geographically weighted regression approach. *Forest Science and Technology*, *21*(1), 38–50. https://doi.org/10.1080/21580103.2024.2438602

Rasyid, A., As, M. A., Nurdin, N., Jaya, I., & Ibrahim. (2016). Impact of human interventions on mangrove ecosystem in spatial perspective. *Iop Conference Series Earth and Environmental Science*, *47*(1). https://doi.org/10.1088/1755-1315/47/1/012041

Richards, D. and Friess, D. (2015). Rates and drivers of mangrove deforestation in Southeast Asia, 2000–2012. Proceedings of the National Academy of Sciences, 113(2), 344-349. https://doi.org/10.1073/pnas.1510272113

Salim, H. L., Adi, N. S., Kepel, T. L., & Ati, R. N. A. (2020, August). Estimating mangrove biomass using drone in Karimunjawa Islands. In IOP Conference Series: Earth and Environmental Science (Vol. 561, No. 1, p. 012054). IOP Publishing. https://doi.org/10.1088/1755-1315/561/1/012054

Salle, S., Soma, A., Paembonan, S., & Rahmat, S. (2024). Social Interaction Dynamics and Mangrove Ecosystem Management for Blue Carbon, Case Study: Tongke-tongke Mangrove Tourism area Indonesia. Iop Conference Series Earth and Environmental Science, 1430(1), 012025. https://doi.org/10.1088/1755-1315/1430/1/012025

Sidik, F., Kusuma, D. W., Priyono, B., Proisy, C., & Lovelock, C. E. (2020). Managing sediment dynamics through reintroduction of tidal flow for mangrove restoration in abandoned aquaculture ponds. In *Dynamic Sedimentary Environments of Mangrove Coasts*. https://doi.org/10.1016/B978-0-12-816437-2.00004-5

Solihuddin, T., Triana, K., Rachmayani, R. et al. The impact of coastal erosion on land cover changes in Muaragembong, Bekasi, Indonesia: a spatial approach to support coastal conservation. J Coast Conserv 28, 43 (2024). https://doi.org/10.1007/s11852-024-01045-2

Tanur, E. A., Imran, H. A., Angrianto, R., May, N. L., & Anwar, A. (2024). Impact Analysis of Human Activities on Mangrove Conservation in Coastal Sulawesi. West Science Nature and Technology, 2(01), 1-8. https://doi.org/10.58812/wsnt.v2i04.742

Utomo, D. P., Handayani, T., Susiloningtyas, D., & Mansessa, M. D. M. (2021). The spatial dynamics of mangrove forest in the Alas Purwo Banyuwangi National Park marine tourism area using remote sensing images. In W. Oktavia, R. Amrulloh, & E. Tampubolon (Eds.), *IOP Conference Series: Earth and Environmental Science* (Vol. 771, Number 1). IOP Publishing Ltd. https://doi.org/10.1088/1755-1315/771/1/012012

Vitasari, M. (2015). Kerentanan Ekosistem Mangrove terhadap Ancaman Gelombang Ektrim/Abrasi Di Kawasan Konservasi Pulau Dua Banten. Bioedukasi: Jurnal Pendidikan Biologi, 8(2), 33. https://doi.org/10.20961/bioedukasi-uns.v8i2.3870

Walcker, R., Gandois, L., Proisy, C., Corenblit, D., Mougin, É., Laplanche, C., Ray, R., & Fromard, F. (2018). Control of “blue carbon” storage by mangrove ageing: Evidence from a 66-year chronosequence in French Guiana. *Global Change Biology*, *24*(6), 2325–2338. https://doi.org/10.1111/gcb.14100

Yamamoto, Y. (2023). Living under ecosystem degradation: Evidence from the mangrove–fishery linkage in Indonesia. *Journal of Environmental Economics and Management*, *118*. https://doi.org/10.1016/j.jeem.2023.102788

Yang, Y., Meng, Z., Zu, J., Cai, W., Wang, J., Su, H., & Yang, J. (2024). Fine-Scale Mangrove Species Classification Based on UAV Multispectral and Hyperspectral Remote Sensing Using Machine Learning. *Remote Sensing*, *16*(16), 3093. https://doi.org/10.3390/rs16163093

Zapf, A., Castell, S., Morawietz, L., & Karch, A. (2016). *Measuring inter-rater reliability for nominal data–which coefficients and confidence intervals are appropriate?* https://link.springer.com/article/10.1186/s12874-016-0200-9